Journal of Engineering Science *Vol. XXXIII, no. 1 (2026), pp. 21 - 36*
Fascicle *Industrial Engineering* *ISSN 2587-3474*
Topic *Materials Science and New Technologies* *eISSN 2587-3482*

https://doi.org/10.52326/jes.utm.2026.33(1).02
UDC 544.6:621.382: 539.2

THEORETICAL PRINCIPLES GOVERNING ELECTROCHEMICAL IMPEDANCE SPECTROSCOPY IN NANOSTRUCTURED SEMICONDUCTOR ELECTRODES

Simon Busuioc*, ORCID: 0009-0006-2601-4015

National Center for Materials Study and Testing, Technical University of Moldova, Stefan cel Mare Blvd. 168, Chisinau, MD-2004, Republic of Moldova
* Corresponding author: Simon Busuioc, *simon.busuioc@cnstm.utm.md*

Received: 12. 18. 2025
Accepted: 25. 01. 2026

Abstract. Electrochemical impedance spectroscopy (EIS) provides a powerful means of probing interfacial and charge-transport phenomena in semiconductor electrodes, yet interpretation becomes increasingly difficult when applied to nanostructured materials. Semiconductor nanowires, nanotubes, and porous films exhibit high surface areas, heterogeneous morphologies, and defect-rich interfaces, all of which modify their impedance response. Theoretical principles regarding EIS behavior in such systems are presented, beginning with semiconductor–electrolyte junction formation, space-charge layer development, band bending and the influence of surface states. Key elements of equivalent-circuit descriptions are examined, including double-layer capacitance, charge-transfer resistance and diffusion-related impedance contributions. Special emphasis is placed on constant-phase elements and distributed models required to capture non-ideal capacitive behavior characteristic of nanoscale electrodes. Common challenges in spectral interpretation, such as overlapping time constants, non-uniform current distribution and deviations from classical Randles-type responses, are summarized within a unified theoretical framework to support reliable modelling and analysis.

Keywords: *Electrochemical response, nanostructured semiconductors, space-charge layer, charge-transfer resistance, equivalent circuit.*

Rezumat. Spectroscopia de impedanță electrochimică (EIS) reprezintă un instrument puternic pentru investigarea fenomenelor interfaciale și a transportului de sarcină în electrozii semiconductori, însă interpretarea devine semnificativ de complexă în cazul materialelor nanostructurate. Nanofirele, nanotuburile și peliculele poroase pe bază de semiconductori se caracterizează prin suprafețe mari, morfologii heterogene și interfețe bogate în defecte, factori care influențează profund răspunsul în impedanță. În această lucrare sunt expuse principiile teoretice esențiale ale comportamentului EIS în astfel de sisteme, începând cu formarea joncțiunii semiconductor–electrolit, dezvoltarea stratului de sarcină spațială, îndoirea benzilor de energie și influența stărilor de suprafață. Sunt analizate elementele cheie ale circuitelor echivalente — inclusiv capacitatea dublu strat, rezistența la transfer de sarcină și contribuțiile impedanței asociate cu difuziunea. Se acordă o atenție specială elementelor cu fază constantă (CPE) și modelelor de circuit care descriu diferențele spațiale ale

proprietăților electrochimice pe diferite regiuni ale structurii electrodului, necesare pentru a surprinde comportamentul capacitiv neideal caracteristic electrozilor la scala nanometrică. Provocările comune în interpretarea spectrelor, precum constantele de timp suprapuse, distribuția neuniformă a curentului și abaterile față de răspunsurile clasice de tip Randles, sunt integrate într-un cadru teoretic unitar pentru a susține o modelare și analiză fiabilă.

Cuvinte-cheie: *răspuns electrochimic, semiconductori nanostructurați, strat de sarcină spațială, rezistență la transferul de sarcină, circuit echivalent.*

1. Introduction

Electrochemical impedance spectroscopy (EIS) is widely used to investigate interfacial charge-transfer processes, mass transport, and adsorption phenomena in electrochemical systems [1]. The technique allows separation of these processes according to their characteristic time constants, thereby yielding quantitative parameters such as charge-transfer resistance, double-layer capacitance, and diffusion coefficients. Historically, EIS models and equivalent-circuit interpretations have been developed primarily for metallic or macroscopically homogeneous electrodes, where relatively simple charge-transfer and transport mechanisms dominate the interfacial response [2].

Electrochemical methods offer a broad range of applications in the processing and modification of semiconductor materials. Electrochemical etching is commonly used for the controlled formation of porous semiconductors, resulting in porous layers with tunable morphology and porosity [3–9], or, in more advanced cases, nanowire and nanochannel networks that can exhibit partial or preferential alignment relative to the substrate [3], [10] Such structures are particularly attractive due to their high surface area and the possibility of controlling charge transport pathways through geometrical design. In addition, electrochemical deposition represents a versatile and cost-effective approach for the fabrication of hybrid structures based on semiconductor materials, enabling the localized deposition of metallic nanodots or thin metallic phases onto semiconductor surfaces [11], [12]. This approach allows control over particle size, distribution, and surface coverage, which is essential for tuning interfacial properties and functional performance in applications such as sensing, catalysis, and energy-related devices.

Nanostructured semiconductor electrodes—such as metal-oxide nanowires, nanotubes, and porous films—introduce considerably greater complexity owing to their high surface-to-volume ratios, morphological heterogeneity, and intrinsic semiconductor electronic properties.

Phenomena including space-charge regions, surface defect states, and band bending strongly affect the impedance response and frequently cause deviations from ideal capacitive or diffusive behavior [13–15]. Nanoscale transport pathways distributed active sites, and geometric non-uniformity commonly give rise to depressed semicircles, non-integer phase angles, and overlapping relaxation-time distributions in the recorded spectra [16].

Reliable interpretation of such spectra requires theoretical frameworks that combine semiconductor physics with established impedance-modelling tools, incorporating elements such as space-charge capacitance, surface-state contributions, diffusion/reaction elements, and distributed or transmission-line representations.

This review study provides a structured overview of these theoretical principles, with emphasis on their application to the accurate analysis and modelling of impedance data obtained from nanostructured semiconductor electrodes.

2. Semiconductor–Electrolyte Interface Theory

The interface between a semiconductor electrode and an electrolyte plays a primary role in determining the electrochemical impedance response. At the interface, the semiconductor's energy levels adjust to match the electrochemical potential of the electrolyte, leading to the formation of a space-charge region within the semiconductor [17]. The width and properties of this region depend on the doping type, doping concentration, applied potential, and surface states present on the electrode. A simple scheme is represented in Figure 1.

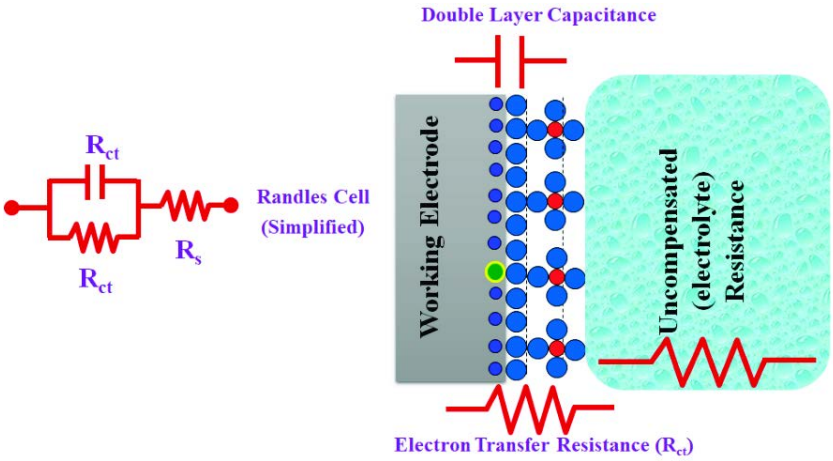

Figure 1. Illustration of the Randles circuit and double-layer structure.
Reproduced from [2] *Electrochemical Impedance Spectroscopy (EIS): Principles, Construction, and Biosensing Applications. Sensors*, 2021, 21, 6578, under **CC BY 4.0**.
https://doi.org/10.3390/s21196578

2.1 Space-Charge Layer Formation

For an n-type semiconductor in contact with an electrolyte, the Fermi level of the semiconductor adjusts to achieve equilibrium with the redox potential of the solution. This equilibration results in band bending near the surface, creating a depletion or accumulation layer depending on the relative energy levels [18]. The space-charge capacitance, C_{sc}, associated with this layer can be expressed using the Mott–Schottky relation:

$$\frac{1}{C_{sc}^2} = \frac{2}{\varepsilon\varepsilon_0 e N_D}\left(V - V_{fb} - \frac{k_B T}{e}\right) \quad (1)$$

where:

- C_{sc} is the space-charge capacitance (F·m^{-2}),
- ε is the semiconductor dielectric constant,
- ε_0 is the vacuum permittivity,
- e is the elementary charge,
- N_D is the donor density for n-type semiconductors,
- V is the applied potential,
- V_{fb} is the flat-band potential,
- k_B is the Boltzmann constant,
- T is the absolute temperature.

This equation establishes a direct relationship between the measured capacitance and the semiconductor doping density, enabling analysis of electronic properties from EIS measurements as seen in Figure 2 [19].

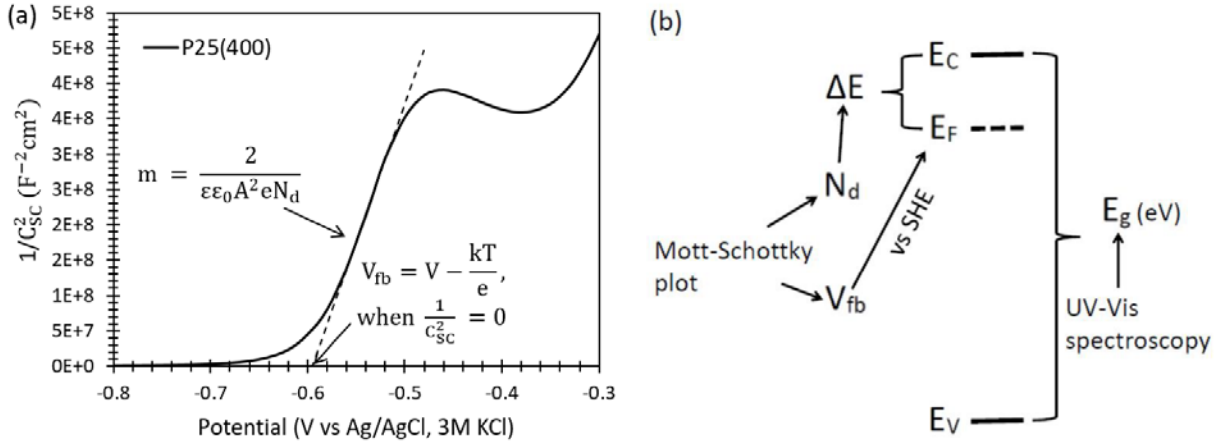

Figure 2. Mott–Schottky analysis and band edge diagram for TiO_2.
Reproduced from [20] *Effects of Mott–Schottky Frequency Selection and Other Controlling Factors on Flat-Band Potential and Band-Edge Position Determination of TiO_2. Catalysts*, 2023, 13, 1000, under **CC BY 4.0**.
https://doi.org/10.3390/catal13061000.

2.2 Influence of Surface States

Surface states, arising from defects, dangling bonds, or adsorbed species, introduce additional energy levels within the bandgap of the semiconductor. These states can trap charge carriers, leading to non-ideal capacitance behavior and frequency-dependent responses in impedance spectra [21]. The contribution of surface states, C_{ss}, can be incorporated into the total interfacial capacitance, C_{int}, as [22]:

$$\frac{1}{C_{int}} = \frac{1}{C_{sc}} + \frac{1}{C_{ss}} + \frac{1}{C_{dl}} \quad (2)$$

where C_{dl} is the double-layer capacitance formed at the semiconductor–electrolyte interface.

2.3 Bending and Charge-Transfer Kinetics

Band bending at the semiconductor surface directly influences the rate of electron transfer across the interface. A higher degree of band bending can increase the effective barrier for charge transfer, thereby increasing the observed charge-transfer resistance, R_{ct}, in EIS spectra [23]. For a simple redox reaction at the interface, the charge-transfer resistance can be related to the exchange current density, i_0, via [22]:

$$R_{ct} = \frac{RT}{nFi_0} \quad (3)$$

where:

- R is the universal gas constant,
- T is the temperature,
- n is the number of electrons involved,
- F is the Faraday constant,
- i_0 is the exchange current density.

Surface states and nano structuring can modify i_0 and introduce distributed kinetics, which are often represented in EIS by constant-phase elements (CPE) instead of ideal capacitors [23].

3. Double-Layer Capacitance and Charge Transfer Resistance

The electrochemical response of nanostructured semiconductor electrodes is largely determined by interfacial capacitance and charge-transfer kinetics. At the electrode–

electrolyte interface, ions in the electrolyte form an electrical double layer (EDL) adjacent to the semiconductor surface. This layer acts as a capacitance, commonly denoted as the double-layer capacitance, C_{dl}, and contributes directly to the impedance spectrum [24].

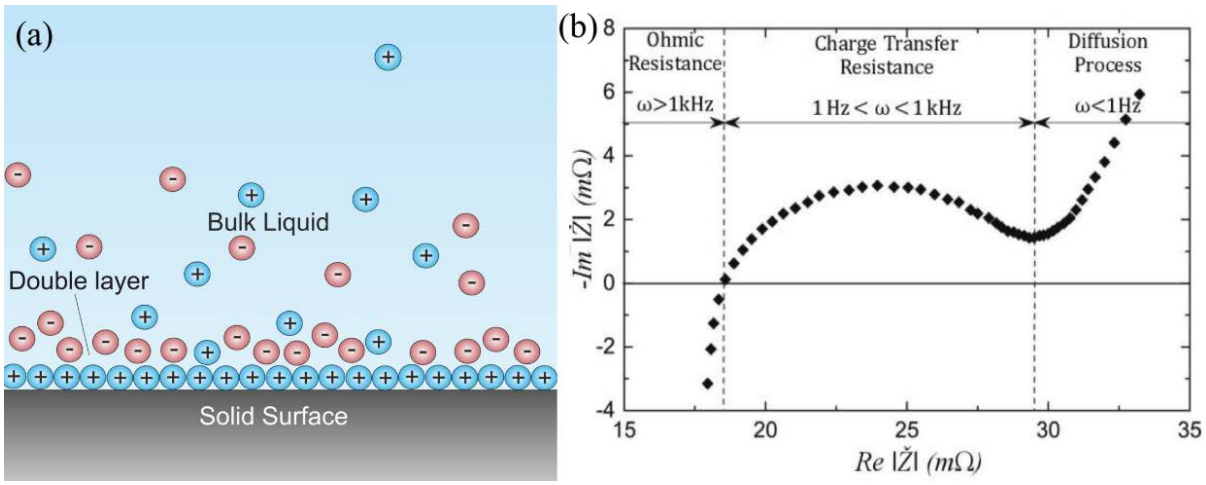

Figure 3. a) Schematic representation of the electrical double layer at a solid–liquid interface.

Source: *Double Layer* by *Gringer*, licensed under **CC BY-SA 3.0**. https://commons.wikimedia.org/wiki/File:Double_Layer.png. b) Nyquist plot indicating ohmic resistance, charge-transfer resistance, and diffusion processes.

Reproduced from [25] *Impact of Relaxation Time on Electrochemical Impedance Spectroscopy Characterization of the Most Common Lithium Battery Technologies—Experimental Study and Chemistry-Neutral Modeling. Smart Cities*, 2023, 12, 77, under **CC BY 4.0**. https://doi.org/10.3390/wevj12020077

3.1 Double-Layer Capacitance

The double-layer capacitance (Figure 3a) arises due to separation of charges at the interface and is classically modeled by the Helmholtz or Gouy–Chapman theories [26, 27]. The Helmholtz model describes a compact layer of ions of thickness $d$at the electrode surface:

$$C_{dl} = \frac{\varepsilon\varepsilon_0}{d} \tag{4}$$

where:

- $C_{dl}$is the double-layer capacitance (F·m^{-2}),
- $\varepsilon$is the dielectric constant of the electrolyte,
- $\varepsilon_0$is the vacuum permittivity,
- $d$is the effective thickness of the Helmholtz layer.

For nanostructured electrodes, deviations from ideal capacitive behavior often occur due to surface roughness, heterogeneous morphology, and porous architectures [28]. These deviations are frequently represented in EIS spectra using constant-phase elements (CPE), which account for non-ideal frequency-dependent behavior:

$$Z_{CPE} = \frac{1}{Q(j\omega)^n} \tag{5}$$

where:

- $Z_{CPE}$is the impedance of the CPE,
- $Q$is the CPE parameter related to capacitance,
- $j$is the imaginary unit,

- $\omega$is the angular frequency,
- $n$is an exponent (0 < n≤ 1), representing deviation from ideal capacitive behaviour.

3.2 Charge-Transfer Resistance

Charge-transfer resistance, R_{ct}, (Figure 3b) quantifies the resistance to electron transfer across the electrode–electrolyte interface. It is inversely proportional to the exchange current density, i_0, of the redox reaction occurring at the interface [29]:

$$R_{ct} = \frac{RT}{nFi_0} \tag{6}$$

where:

- $R$is the universal gas constant (J·mol^{-1}·K^{-1}),
- $T$is the absolute temperature (K),
- $n$is the number of electrons transferred,
- $F$is the Faraday constant (C·mol^{-1}),
- $i_0$is the exchange current density (A·m^{-2}).

In nanostructured electrodes, the effective R_{ct}may vary across the surface due to differences in local conductivity, surface states, and electronic defects, which can introduce distributed kinetics. In EIS spectra, charge-transfer resistance typically manifests as the diameter of the semicircular region in the Nyquist plot. Non-uniform electrode surfaces often produce depressed semicircles, which are effectively modeled using CPEs in parallel with R_{ct} [30].

3.3 Interplay Between Double-Layer Capacitance and Charge-Transfer Resistance

The overall impedance of the electrode–electrolyte interface is determined by the combined effects of double-layer capacitance and charge-transfer resistance. In the simplest form, this combination is represented by the parallel configuration of $C_{dl}$and R_{ct}, often included in the classical Randles equivalent circuit:

$$Z_{interface} = R_s + \frac{1}{\frac{1}{R_{ct}} + j\omega C_{dl}} \tag{7}$$

where R_s is the series resistance of the electrolyte and contacts. For nanostructured electrodes, distributed capacitances, surface heterogeneity, and deviations from ideal behaviour necessitate the use of CPEs or extended transmission-line models for accurate representation [23].

4. Equivalent Circuit Models

The interpretation of electrochemical impedance spectroscopy (EIS) (Figure 4a) data relies heavily on the use of equivalent circuit models that translate frequency-domain measurements into physically meaningful parameters. For semiconductor electrodes, equivalent circuits must incorporate contributions from double-layer capacitance, charge-transfer resistance, space-charge capacitance, surface states, and diffusion processes. The choice of circuit depends on electrode morphology, surface heterogeneity, and the degree of non-ideal behavior observed in impedance spectra [23].

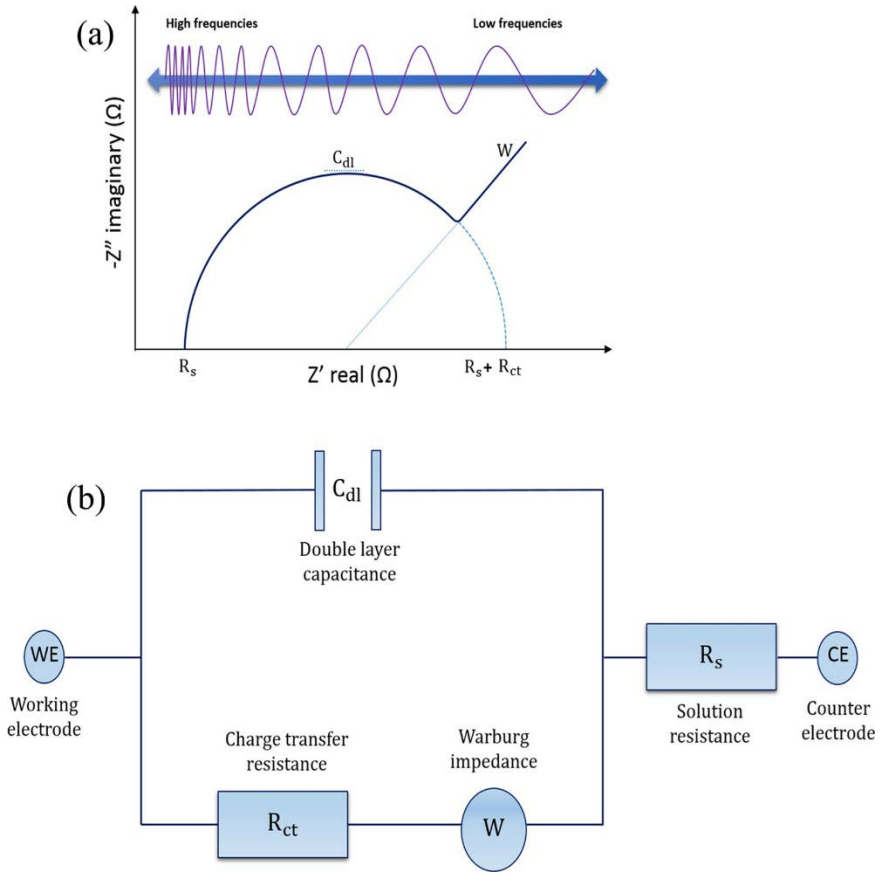

Figure 4. General scheme of a Nyquist plot and Randles' equivalent circuit (showing R_s, R_{ct}, $C_{dl}$and Warburg W).

Adapted from [31] *A review on impedimetric immunosensors for pathogen and biomarker detection. Medical Microbiology and Immunology* 209:343–362 (2020), under **CC BY 4.0**.
https://doi.org/10.1007/s00430-020-00668-0

4.1 Classical Randles Circuit

The Randles circuit (Figure 4b) represents the simplest model for an electrochemical interface, consisting of the series resistance of the electrolyte (R_s) in series with a parallel combination of the charge-transfer resistance (R_{ct}) and the double-layer capacitance (C_{dl}):

$$Z(\omega) = R_s + \frac{1}{\frac{1}{R_{ct}} + j\omega C_{dl}} \tag{8}$$

where $\omega$is the angular frequency. In EIS spectra, the diameter of the semicircle in the Nyquist plot corresponds to R_{ct}, while C_{dl} determines the curvature of the semicircle. For ideal electrodes, the Randles model accurately describes the high- and mid-frequency response, but deviations appear for nanostructured systems due to surface heterogeneity [9, 16].

4.2 Constant-Phase Element (CPE)

Nanostructured semiconductor electrodes often exhibit non-ideal capacitive behavior due to surface roughness, distributed reaction sites, or inhomogeneous conductivity. These effects are represented in equivalent circuits by a constant-phase element (CPE), whose impedance is given by [32]:

$$Z_{CPE} = \frac{1}{Q(j\omega)^n} \tag{9}$$

where:

- $Q$is a CPE constant related to capacitance,
- n($0 < n \leqslant 1$) quantifies the deviation from ideal behaviour.

When $n = 1$, the CPE reduces to an ideal capacitor; when $n < 1$, it models a distributed or non-uniform capacitance commonly observed in nanostructured electrodes [2].

4.3 Warburg Impedance

Diffusion-controlled processes in electrochemical systems contribute a frequency-dependent impedance, known as Warburg impedance (Z_W). For semi-infinite linear diffusion, $Z_W$is expressed as:

$$Z_W = \sigma \frac{1-j}{\sqrt{\omega}} \tag{10}$$

where $\sigma$is the Warburg coefficient, dependent on the diffusion coefficient and concentration of electroactive species.

For finite-length diffusion (e.g., in nanowire arrays), the Warburg element is modified to account for boundary conditions:

$$Z_W = R_W \frac{\tanh(j\omega\tau_D)^{1/2}}{(j\omega\tau_D)^{1/2}} \tag{11}$$

where $\tau_D$is the diffusion time constant.

Warburg elements typically appear in the low-frequency region of EIS spectra, manifesting as linear tails in Nyquist plots [2].

4.4 Distributed Transmission-Line Models

For high-aspect-ratio nanostructures such as nanowires, nanotubes, and porous films, interfacial and bulk resistances and capacitances are distributed along the electrode structure. Transmission-line models represent the electrode as a series of infinitesimal resistive and capacitive elements, capturing the spatial distribution of impedance contributions:

$$Z_{TL} = \sqrt{\frac{R_b+R_{ct}}{j\omega C_{dl}}} \coth[\sqrt{(R_b + R_{ct})j\omega C_{dl}}] \tag{12}$$

where $R_b$is the bulk resistance of the electrode.

Transmission-line circuits provide a more realistic representation of the frequency response for nanostructured electrodes than lumped-element models, particularly when multiple processes overlap [33].

5. Frequency-Dependent Behavior of Nanostructured Electrodes

Electrochemical impedance spectroscopy (EIS) characterizes electrochemical systems by measuring their response over a range of frequencies. In nanostructured semiconductor electrodes, the impedance response is governed by a combination of double-layer capacitance, charge-transfer resistance, space-charge capacitance, surface states, and diffusion processes, each dominating specific frequency regions [34].

5.1 High-Frequency Region

At high frequencies (typically >10 kHz), the impedance response is dominated by the series resistance (R_s) of the electrolyte and contacts, as well as the interfacial capacitances. In nanostructured electrodes, this region is particularly sensitive to the distributed double-

layer capacitance (C_{dl}) and space-charge capacitance (C_{sc}). Non-uniform surfaces or high surface-area architectures can produce depressed semicircles in Nyquist plots, reflecting non-ideal capacitive behavior represented by constant-phase elements (CPEs) [2].

5.2 Mid-Frequency Region

The mid-frequency range (typically 10 Hz–10 kHz) is predominantly influenced by charge-transfer resistance (R_{ct}) at the semiconductor–electrolyte interface. The parallel combination of R_{ct} and interfacial capacitances produces semicircular features in Nyquist plots, whose diameter corresponds to the magnitude of R_{ct}. In nanostructured electrodes, distributed reaction sites and surface states can broaden or depress the semicircle, requiring CPEs in parallel with R_{ct} for accurate modelling [35].

5.3 Low-Frequency Region

At low frequencies (<10 Hz), mass transport and diffusion processes dominate. The Warburg impedance (Z_W) represents semi-infinite linear diffusion, producing a 45° linear segment in the Nyquist plot. For nanostructured electrodes with finite-length diffusion paths, the Warburg element exhibits frequency-dependent saturation, and the linear region bends toward a vertical line at very low frequencies, indicating diffusion limitations [36]. Transmission-line models effectively capture these spatially distributed diffusion effects, particularly in high-aspect-ratio nanostructures such as nanowire arrays.

5.4 Bode Plot Interpretation

Bode plots provide additional insight by representing the magnitude and phase of impedance as functions of frequency. High-frequency peaks in phase plots correspond to capacitive behavior of the double-layer and space-charge regions, while mid-frequency peaks indicate the presence of charge-transfer processes. Low-frequency tails reflect diffusion-controlled kinetics. Nanostructured electrodes often exhibit multiple overlapping peaks due to distributed capacitances and inhomogeneous reaction rates, which can complicate simple Randles-type interpretations [35].

5.5 Distributed Effects and Non-Ideal Behavior

Nano structuring introduces heterogeneity, resulting in non-ideal, frequency-dependent behavior that cannot be accurately captured by simple lumped-element circuits. Constant-phase elements, transmission-line models, and distributed Warburg elements are required to account for these effects. Proper analysis of frequency-dependent responses allows for separation of capacitive, resistive, and diffusive contributions, facilitating a mechanistic understanding of electrochemical processes in nanostructured semiconductor electrodes [37].

6. Diffusion and Warburg Impedance

Diffusion processes play a crucial role in the low-frequency behavior of electrochemical systems, particularly in nanostructured semiconductor electrodes where transport pathways are often spatially constrained. The Warburg impedance (Z_W) is commonly employed to describe frequency-dependent diffusion phenomena in electrochemical impedance spectroscopy (EIS) [37].

6.1 Semi-Infinite Linear Diffusion

For semi-infinite diffusion, where the diffusion layer is effectively unlimited compared to the electrode dimensions, the Warburg impedance is defined as [38]:

$$Z_W = \sigma \frac{1-j}{\sqrt{\omega}} \quad (13)$$

where:

- $Z_W$is the Warburg impedance (Ω),
- $\sigma$is the Warburg coefficient, dependent on the diffusion coefficient $D$and concentration of electroactive species C^*,
- $j$is the imaginary unit,
- $\omega$is the angular frequency (rad·s^{-1}).

The Warburg coefficient σcan be expressed as [38]:

$$\sigma = \frac{RT}{n^2F^2A\sqrt{2DC^*}} \quad (14)$$

where:

- $R$is the universal gas constant (J·mol^{-1}·K^{-1}),
- $T$is the absolute temperature (K),
- $n$is the number of electrons transferred,
- $F$is the Faraday constant (C·mol^{-1}),
- $A$is the electrode surface area (m^2),
- $D$is the diffusion coefficient (m^2·s^{-1}),
- $C^*$is the bulk concentration of the redox species (mol·m^{-3}).

In Nyquist plots, semi-infinite diffusion manifests as a 45° linear segment at low frequencies, indicating a balance between resistive and capacitive contributions from ion transport.

6.2 Finite-Length Diffusion

In nanostructured electrodes, diffusion paths are often limited by nanoscale geometry, electrode thickness, or porous architecture. Finite-length diffusion modifies the Warburg impedance according to the following expression [39]:

$$Z_W = R_W \frac{\tanh((j\omega\tau_D)^{1/2})}{(j\omega\tau_D)^{1/2}} \quad (15)$$

where:

- $R_W$is the Warburg resistance,
- $\tau_D = \frac{L^2}{D}$is the diffusion time constant,
- $L$is the effective diffusion length.

This formulation accounts for saturation of the Warburg impedance at very low frequencies, which appears as a bending of the 45° line toward the vertical axis in Nyquist plots. Such behavior is particularly relevant for arrays of nanowires, nanotubes, and porous films, where diffusion limitations can dominate low-frequency impedance [40].

6.3 Integration with Equivalent Circuits

Warburg elements are commonly incorporated into equivalent circuits to model diffusion-limited processes. In the classical Randles circuit, a semi-infinite Warburg element (Z_W) is connected in series with $R_{ct}$and parallel to C_{dl}:

$$Z_{total} = R_s + \frac{1}{\frac{1}{R_{ct}+Z_W} + j\omega C_{dl}} \quad (16)$$

For nanostructured electrodes, transmission-line models or distributed Warburg elements are preferred to account for spatial heterogeneity and overlapping time constants [38].

6.4 Implications for Nanostructured Electrodes

Diffusion processes in nanostructured electrodes are strongly affected by geometry, pore size, and electrode thickness. The Warburg impedance provides a quantitative tool to evaluate diffusion coefficients, effective path lengths, and limitations in ion transportation. Correct modeling of Warburg contributions is essential for separating resistive, capacitive, and diffusion-controlled components of impedance spectra, enabling accurate interpretation of electrochemical kinetics at the nanoscale.

7. Modeling Impedance of Semiconductor Nanostructures

The accurate modeling of electrochemical impedance spectra in semiconductor nanostructures requires integration of interfacial capacitances, charge-transfer resistance, and diffusion contributions, while accounting for the spatial heterogeneity and nanoscale morphology of the electrode [37]. Nanostructured electrodes, including metal-oxide nanowires, nanotubes, and porous films, exhibit distributed electrical properties that cannot be fully represented by classical lumped-element circuits [41].

7.1 Distributed Equivalent-Circuit Models

For nanostructured electrodes, distributed equivalent-circuit models are employed to represent spatially varying resistive and capacitive elements. Transmission-line models, often composed of repeated series combinations of resistance (R_b), charge-transfer resistance (R_{ct}), and double-layer or space-charge capacitance (C_{dl} or C_{sc}), provide a more realistic description:

$$Z_{TL} = \sqrt{\frac{R_b+R_{ct}}{j\omega C_{dl}}}\coth[\sqrt{(R_b + R_{ct})j\omega C_{dl}}] \quad (17)$$

where $R_b$is the bulk resistance of the electrode and cothdenotes the hyperbolic cotangent function. These models capture frequency-dependent behavior resulting from the extended geometry and heterogeneity of nanoscale electrodes [42].

7.2 Integration of Space-Charge and Surface-State Effects

Space-charge regions and surface states significantly influence the interfacial impedance of semiconductor electrodes. The total interfacial capacitance, C_{int}, is expressed as a series combination of space-charge capacitance (C_{sc}), surface-state capacitance (C_{ss}), and double-layer capacitance (C_{dl}) as mentioned in Equation (2). The incorporation of C_{ss} is particularly important for nanostructured electrodes where surface defects and adsorbed species are abundant. Non-ideal behavior introduced by surface-state distribution can be represented using constant-phase elements (CPE) to accurately model the frequency-dependent response [43].

7.3 Modeling Charge-Transfer and Diffusion Processes

Charge-transfer resistance (R_{ct}) and diffusion-controlled impedance (Warburg element, Z_W) are combined in equivalent circuits to capture mid- and low-frequency spectral features. For nanostructured electrodes, overlapping time constants from distributed $R_{ct}$and finite-length diffusion paths necessitate modified Warburg elements or transmission-line approaches:

$$Z_{total} = R_s + \frac{1}{\frac{1}{R_{ct}+Z_W}+(j\omega C_{dl})^n} \quad (18)$$

where n represents the exponent of the CPE, reflecting non-ideal capacitive behavior.
This formulation enables deconvolution of contributions from charge-transfer kinetics, interfacial capacitances, and diffusion phenomena [35].

7.4 Challenges in Modeling Nanostructured Impedance

Accurate modeling of nanostructured semiconductor electrodes is complicated by several factors [44]:

1. Surface heterogeneity: Nanostructured electrodes contain distributed active sites, which produce non-uniform charge-transfer kinetics.
2. Overlapping time constants: Multiple processes may occur over similar frequency ranges, complicating spectral interpretation.
3. Non-ideal capacitive behavior: High surface area and roughness result in frequency-dependent capacitance, requiring CPE modeling.
4. Finite diffusion paths: Diffusion limitations in nanowires, nanotubes, and porous electrodes produce deviations from classical Warburg behavior.

Addressing these challenges requires careful selection of equivalent-circuit elements and fitting strategies, combined with theoretical understanding of semiconductor electrochemistry at the nanoscale.

8. Limitations of EIS Interpretation in Nanomaterials

Electrochemical impedance spectroscopy (EIS) is useful tool for probing interfacial processes and charge transport in semiconductor electrodes. However, its interpretation in nanostructured materials is subject to several inherent limitations due to the complexity of nanoscale morphologies, distributed kinetics, and non-ideal capacitive behavior [45].

Nanostructured electrodes often display non-ideal capacitive responses arising from surface roughness, porosity, and heterogeneous distributions of surface states. Constant-phase elements (CPEs) are commonly used to model these deviations; however, the physical interpretation of CPE parameters is not straightforward. The exponent $n$in a CPE reflects the degree of deviation from ideal capacitance, but it does not directly quantify specific physical features such as pore size, surface roughness, or defect density. Consequently, extrapolating mechanistic insights solely from CPE parameters may be ambiguous [46].

Multiple electrochemical processes, including double-layer charging, charge transfer, and diffusion, may occur over similar frequency ranges in nanostructured electrodes. Overlapping time constants complicate the separation of individual contributions and can lead to misinterpretation of impedance spectra. In particular, mid-frequency semicircles may contain contributions from both $R_{ct}$and space-charge effects, while low-frequency tails may simultaneously reflect diffusion and adsorption processes [35].

Finite diffusion lengths in nanowire arrays, nanotubes, and porous films introduce deviations from classical semi-infinite Warburg behavior. Standard Warburg models may underestimate the impact of restricted diffusion or misrepresent the low-frequency impedance, leading to inaccurate extraction of diffusion coefficients. Transmission-line models offer improvements but still require assumptions regarding uniformity of nanostructure dimensions and porosity [35].

Nanostructured electrodes exhibit spatial variations in doping, morphology, and electronic properties. These inhomogeneities create distributed resistive and capacitive

behavior that cannot be fully captured by simple equivalent circuits. Fitting EIS data to classical models without accounting for heterogeneity may produce parameters that lack direct physical meaning or predictive power [47].

Accurate EIS interpretation also depends on experimental factors such as temperature stability, electrode preparation, electrolyte composition, and instrumentation limitations. Noise, parasitic inductance, and limited frequency range can obscure or distort impedance features, further complicating analysis in nanoscale systems [2].

Conclusions

Electrochemical impedance spectroscopy is a powerful way to study what happens at the interface of nanostructured semiconductor electrodes. The overall impedance comes from several factors working together: the double-layer capacitance, charge-transfer resistance, space-charge capacitance, surface states, and different types of diffusion. Because nano structuring creates complexity and non-ideal behavior, researchers often rely on constant-phase elements (CPEs), Warburg elements, and distributed or transmission-line equivalent circuits to describe the system accurately.

At high frequencies, the response is mainly shaped by interfacial and space-charge capacitances. In the mid-frequency range, charge-transfer reactions dominate. At low frequencies, diffusion processes take over—and in nanostructured materials, the limited diffusion length means that classic Warburg models often need to be adjusted. Transmission-line models are especially helpful here because they can represent spatial variations and the overlapping time constants that commonly appear in nanowires, nanotubes, and porous electrodes.

Still, interpreting EIS data for nanostructured electrodes isn't always straightforward. Non-ideal capacitive behavior, overlapping timescales, restricted diffusion, and surface irregularities can make analysis tricky. Getting reliable electrochemical parameters requires thoughtful experimental design, choosing the right equivalent-circuit model, and taking into account the nanoscale structure of the electrode.

Building a solid theoretical understanding of impedance in these systems makes it possible to evaluate interfacial reactions, diffusion limits, and charge-transfer processes with confidence. These insights are valuable for designing advanced electrodes with optimized performance for applications such as energy conversion, catalysis, and sensing.

Funding

This work was funded by Ministry of Education and Research from the Republic of Moldova, institutional subprogram #02.04.02 "Development of technologies and investigation of the properties of layered semiconductor compounds, hybrid nanostructures and laser sources".

Conflicts of Interest

The author declares no conflicts of interest. The funders had no role in the design of the study; in the collection, analyses, or interpretation of data; in the writing of the manuscript; or in the decision to publish the results.

References

1. Zhang H, Sun Z, Sun K, et al (2025) Electrochemical Impedance Spectroscopy-Based Biosensors for Label-Free Detection of Pathogens. Biosensors 15:443. https://doi.org/10.3390/bios15070443

2. Magar HS, Hassan RYA, Mulchandani A (2021) Electrochemical Impedance Spectroscopy (EIS): Principles, Construction, and Biosensing Applications. Sensors 21:6578. https://doi.org/10.3390/s21196578
3. Monaico, E. (2022). Micro- and nano-engineering of III-V and II-VI semiconductor compounds and metal nanostructures based on electrochemical technologies for multifunctional applications. Chișinău: Technical University of Moldova. Available at: http://repository.utm.md/handle/5014/21913
4. Tiginyanu IM, Monaico EV (2024) Self-organized porous semiconductor compounds. In: Encyclopedia of Condensed Matter Physics. Elsevier, pp 350–374. doi: 10.1016/B978-0-323-90800-9.00105-0.
5. Monaico EV, Monaico EI, Ursaki VV, Tiginyanu IM (2023) Porous Semiconductor Compounds with Engineered Morphology as a Platform for Various Applications. Phys Status Solidi RRL – Rapid Res Lett 17:2300039. https://doi.org/10.1002/pssr.202300039
6. Monaico EI, Monaico EV, Ursaki VV, Tiginyanu IM (2021) Evolution of Pore Growth in GaAs in Transitory Anodization Regime from One Applied Voltage to Another. Surf Eng Appl Electrochem 57:165–172. https://doi.org/10.3103/S106837552102006X
7. Monaico E, Tiginyanu I, Ursaki V (2020) Porous semiconductor compounds. Semicond Sci Technol 35:103001. https://doi.org/10.1088/1361-6641/ab9477
8. Monaico EI, Monaico EV, Ursaki VV, Tiginyanu IM (2025) Micro- and Nano-Integration in the Production of GaAs and Ga2O3 Nanowire Arrays by Top-Down Design. J Manuf Mater Process 9:376. https://doi.org/10.3390/jmmp9110376
9. Monaico EV, Tiginyanu IM (2025) How Semiconductor Terminology has Been Enriched by Research of Electrochemical Pore Etching and Electrodeposition. In: Sontea V, Tiginyanu I, Railean S (eds) 7th International Conference on Nanotechnologies and Biomedical Engineering. Springer Nature Switzerland, Cham, pp 311–321. doi: 10.1007/978-3-032-06494-3_31.
10. Monaico EI, Monaico EV, Ursaki VV, Tiginyanu IM (2025) Micro- and Nano-Integration in the Production of GaAs and Ga2O3 Nanowire Arrays by Top-Down Design. J Manuf Mater Process 9:376. https://doi.org/10.3390/jmmp9110376
11. Monaico EV (2024) Micro- and nano-engineering of semiconductor compounds and metal structures based on electrochemical technologies. Ann Acad Romanian Sci Ser Phys Chem 9:85–107. https://doi.org/10.56082/annalsarsciphyschem.2024.1.85
12. Monaico EI, Monaico EV, Ursaki VV, Tiginyanu IM (2022) Controlled Electroplating of Noble Metals on III-V Semiconductor Nanotemplates Fabricated by Anodic Etching of Bulk Substrates. Coatings 12:1521. https://doi.org/10.3390/coatings12101521
13. Krawczyk M, Korbutowicz R, Suchorska-Woźniak P (2024) Impedance Spectroscopy Study of Charge Transfer in the Bulk and Across the Interface in Networked SnO2/Ga2O3 Core–Shell Nanobelts in Ambient Air. Sensors 24:6173. https://doi.org/10.3390/s24196173
14. Busuioc S, Monaico EV (2024) Electrochemical Impedance Spectroscopy for NonEnzymatic Glucose Detection Using ZnO Nanowire Arrays: Substrate Impact Analysis. University Politehnica of Bucharest, Bucharest, Romania, p 30. [Online]. Available: http://www.physics.pub.ro/Site_Conferinta_PM-8/Abstracts_Book.pdf
15. Busuioc S, Monaico EV (2025) Influence of Surface Pre-treatment and Thermal Annealing on the Electrochemical and Wettability Behavior of Copper. In: Sontea V, Tiginyanu I, Railean S (eds) 7th International Conference on Nanotechnologies and Biomedical Engineering. Springer Nature Switzerland, Cham, pp 215–226. doi: 10.1007/978-3-032-06494-3_23.
16. Iram S, Mahmood A, Ehsan MF, et al (2021) Impedance Spectroscopic Study of Nickel Sulfide Nanostructures Deposited by Aerosol Assisted Chemical Vapor Deposition Technique. Nanomaterials 11:1105. https://doi.org/10.3390/nano11051105
17. Leks B, Parzuch A, Nawaz N, et al (2025) Influence of Electrolyte Composition on the Semiconductor–Electrolyte Interface (SEI) Built-In for Enhanced Photoelectrochemical (PEC) Processes. Molecules 30:885. https://doi.org/10.3390/molecules30040885
18. Al-Hilli S, Willander M (2009) The pH Response and Sensing Mechanism of n-Type ZnO/Electrolyte Interfaces. Sensors 9:7445–7480. https://doi.org/10.3390/s90907445
19. Lee SF, Jimenez-Relinque E, Martinez I, Castellote M (2023) Effects of Mott–Schottky Frequency Selection and Other Controlling Factors on Flat-Band Potential and Band-Edge Position Determination of TiO2. Catalysts 13:1000. https://doi.org/10.3390/catal13061000
20. Lee SF, Jimenez-Relinque E, Martinez I, Castellote M (2023) Effects of Mott–Schottky Frequency Selection and Other Controlling Factors on Flat-Band Potential and Band-Edge Position Determination of TiO2. Catalysts 13:1000. https://doi.org/10.3390/catal13061000

21. Brett CMA (2022) Electrochemical Impedance Spectroscopy in the Characterisation and Application of Modified Electrodes for Electrochemical Sensors and Biosensors. Molecules 27:1497. https://doi.org/10.3390/molecules27051497
22. Bard AJ, Faulkner LR (2001) Electrochemical methods: fundamentals and applications, 2. edition. Wiley, New York Weinheim
23. Lazanas A, Prieto Simón B (2025) A Guide to Recognizing Your Electrochemical Impedance Spectra: Revisions of the Randles Circuit in (Bio)sensing. Sensors 25:6260. https://doi.org/10.3390/s25196260
24. Ferre F, Breuiller M, Cedard L (1975) Human placental delta5-3beta hydroxysteroid dehydrogenase activity (delta5-3beta HSDH): intracellular distribution, kinetic properties, retroinhibition and influence of membrane delipidation. Steroids 26:551–570. https://doi.org/10.1016/0039-128x(75)90050-1
25. Hosen MS, Gopalakrishnan R, Kalogiannis T, et al (2021) Impact of Relaxation Time on Electrochemical Impedance Spectroscopy Characterization of the Most Common Lithium Battery Technologies—Experimental Study and Chemistry-Neutral Modeling. World Electr Veh J 12:77. https://doi.org/10.3390/wevj12020077
26. Helmholtz H von (1879) Studien über elektrische Grenzschichten. Ann Phys 243:337–382. https://doi.org/10.1002/andp.18792430702
27. Bolt GH (1955) Analysis of the validity of the Gouy-Chapman theory of the electric double layer. J Colloid Sci 10:206–218. https://doi.org/10.1016/0095-8522(55)90027-1
28. Miszczyk A (2025) Direct Measurement of Effective Electrical Capacitance in Systems with a Constant-Phase Element Behavior Using the Example of Barrier Coatings. Coatings 15:1429. https://doi.org/10.3390/coatings15121429
29. (1924) On the determination of molecular fields. —II. From the equation of state of a gas. Proc R Soc Lond Ser Contain Pap Math Phys Character 106:463–477. https://doi.org/10.1098/rspa.1924.0082
30. Cuevas AL, Dominguez A, Zamudio-García J, et al (2024) Optical and Electrochemical Properties of a Nanostructured ZnO Thin Layer Deposited on a Nanoporous Alumina Structure via Atomic Layer Deposition. Materials 17:1412. https://doi.org/10.3390/ma17061412
31. Leva-Bueno J, Peyman SA, Millner PA (2020) A review on impedimetric immunosensors for pathogen and biomarker detection. Med Microbiol Immunol (Berl) 209:343–362. https://doi.org/10.1007/s00430-020-00668-0
32. Brug GJ, Van Den Eeden ALG, Sluyters-Rehbach M, Sluyters JH (1984) The analysis of electrode impedances complicated by the presence of a constant phase element. J Electroanal Chem Interfacial Electrochem 176:275–295. https://doi.org/10.1016/S0022-0728(84)80324-1
33. De Levie R (1963) On porous electrodes in electrolyte solutions. Electrochimica Acta 8:751–780. https://doi.org/10.1016/0013-4686(63)80042-0
34. Barsoukov E, Macdonald JR (2005) Impedance Spectroscopy: Theory, Experiment, and Applications, 1st ed. Wiley. doi: 10.1002/0471716243.
35. Lazanas ACh, Prodromidis MI (2023) Electrochemical Impedance Spectroscopy—A Tutorial. ACS Meas Sci Au 3:162–193. https://doi.org/10.1021/acsmeasuresciau.2c00070
36. Bumberger AE, Nenning A, Fleig J (2024) Transmission line revisited – the impedance of mixed ionic and electronic conductors. Phys Chem Chem Phys 26:15068–15089. https://doi.org/10.1039/d4cp00975d
37. Da Silva GMG, Faia PM, Mendes SR, Araújo ES (2024) A Review of Impedance Spectroscopy Technique: Applications, Modelling, and Case Study of Relative Humidity Sensors Development. Appl Sci 14:5754. https://doi.org/10.3390/app14135754
38. Nuñez Perez FA (2025) Analytical–Computational Integration of Equivalent Circuit Modeling, Hybrid Optimization, and Statistical Validation for Electrochemical Impedance Spectroscopy. Electrochem 6:35. https://doi.org/10.3390/electrochem6040035
39. Fortuna L, Garraffa G (2025) Characteristic Value Techniques to Approximate Warburg Diffusion Devices. Energies 18:3408. https://doi.org/10.3390/en18133408
40. Lasia A (2014) Electrochemical Impedance Spectroscopy and its Applications. Springer New York, New York, NY Springer New York, 2014. doi: 10.1007/978-1-4614-8933-7.
41. Song J, Bazant MZ (2018) Electrochemical Impedance Imaging via the Distribution of Diffusion Times. Phys Rev Lett 120:. https://doi.org/10.1103/physrevlett.120.116001
42. Costa R, Voroshylova IV, Cordeiro MNDS, et al (2018) Enhancement of differential double layer capacitance and charge accumulation by tuning the composition of ionic liquids mixtures. Electrochimica Acta 261:214–220. https://doi.org/10.1016/j.electacta.2017.12.134

43. Gelderman K, Lee L, Donne SW (2007) Flat-Band Potential of a Semiconductor: Using the Mott–Schottky Equation. J Chem Educ 84:685. https://doi.org/10.1021/ed084p685
44. Fabregat-Santiago F, Bisquert J, Garcia-Belmonte G, et al (2005) Influence of electrolyte in transport and recombination in dye-sensitized solar cells studied by impedance spectroscopy. Sol Energy Mater Sol Cells 87:117–131. https://doi.org/10.1016/j.solmat.2004.07.017
45. Bredar ARC, Chown AL, Burton AR, Farnum BH (2020) Electrochemical Impedance Spectroscopy of Metal Oxide Electrodes for Energy Applications. ACS Appl Energy Mater 3:66–98. https://doi.org/10.1021/acsaem.9b01965
46. Córdoba-Torres P, Mesquita TJ, Nogueira RP (2015) Relationship between the Origin of Constant-Phase Element Behavior in Electrochemical Impedance Spectroscopy and Electrode Surface Structure. J Phys Chem C 119:4136–4147. https://doi.org/10.1021/jp512063f
47. Das S, Banerjee A, Nandi U, Ghosh A (2025) Critical review on the analysis of electrochemical impedance spectroscopy data. J Appl Phys 138:. https://doi.org/10.1063/5.0275205

Citation: Busuioc, S. (2026). Theoretical principles governing electrochemical impedance spectroscopy in nanostructured semiconductor electrodes. *Journal of Engineering Science*. 2026, 33 (1), pp. 21-36. https://doi.org/10.52326/jes.utm.2026.33(1).02.

Submission of manuscripts: jes@meridian.utm.md